PERGAMON

Deep-Sea Research II 49 (2002) 2747–2768

DEEP-SEA RESEARCH
PART II

www.elsevier.com/locate/dsr2

# One-dimensional ecosystem model of the equatorial Pacific upwelling system. Part II: sensitivity analysis and comparison with JGOFS EqPac data

R.C. Dugdale[a,*], R.T. Barber[b], F. Chai[c], T.-H. Peng[d], F.P. Wilkerson[a]

[a] *Romberg Tiburon Center, San Francisco State University, 3152 Paradise Drive, Tiburon CA 94920, USA*
[b] *Duke University, NSOE Marine Laboratory, 135 Duke Marine Lab Road, Beaufort, NC 28516, USA*
[c] *School of Marine Science, 5471 Libby Hall, University of Maine, Orono, ME 04469-5741, USA*
[d] *NOAA Atlantic Oceanographic and Meteorological Laboratory, Ocean Chemistry Division, 4301 Rickenbacker Causeway, Miami, FL 33149-1026, USA*

Received 31 July 2000; received in revised form 26 March 2001; accepted 10 April 2001

**Abstract**

A one-dimensional model of the equatorial Pacific upwelling ecosystem that incorporates two phytoplankton components, two grazers, and three nutrients, $Si(OH)_4$, $NO_3$, and $NH_4$ (Chai et al., Deep-Sea Research II (2002) 2713–2745), was designed to consider the effects of $Si(OH)_4$ limitation on the diatom growth and ecosystem functioning. Model output was obtained for a range of source concentrations of $Si(OH)_4$, 3–15 mmol $m^{-3}$, coinciding with the range measured at 120 m depth during JGOFS EqPac. $NO_3$ was held at 12 mmol $m^{-3}$, reflecting the relatively greater concentrations of $NO_3$ compared to $Si(OH)_4$ in the JGOFS data. The model was shown to function as a chemostat-like system with the loss rates, provided largely from zooplankton grazing, controlling growth rates of the phytoplankton. When different source concentrations of $Si(OH)_4$ were applied, surface concentrations of $Si(OH)_4$ varied within a narrow range compared to $NO_3$ as would occur in a chemostat with limiting $Si(OH)_4$ and non-limiting $NO_3$ in the feed water. Vertical profiles of nutrients compared well with field data. Model results are compared with field data for new and total nitrogen production and export of N, Si, and C, and with other models, although none consider $Si(OH)_4$ specifically. The model suggests that the stability of the equatorial system with its narrow range of biological and chemical variables is conferred by the action of diatoms providing food for mesozooplankton whose grazing also depletes the picoplankton. Diatoms increase with source $Si(OH)_4$ concentrations, and picoplankton population and $NO_3$ consumption decrease, resulting in a maximum surface $TCO_2$ and increased $CO_2$ flux to the atmosphere at intermediate source $Si(OH)_4$ concentrations. Diatoms function in the equatorial system as a silica pump to export silica. This means that sedimented biogenic silica under the equatorial upwelling area should be viewed as an amplifier of changes in surface properties, with important consequences to paleoequatorial productivity. © 2002 Published by Elsevier Science Ltd.

## 1. Introduction

The equatorial Pacific upwelling system is recognized as one of the most important areas of the ocean for global climate effects (Feely et al.,

*Corresponding author.
*E-mail addresses:* rdugdale@sfsu.edu (R.C. Dugdale), rbarber@duke.edu (R.T. Barber), fchai@maine.edu (F. Chai), peng@aoml.noaa.gov (T.-H. Peng), fwilkers@sfsu.edu (F.P. Wilkerson).

0967-0645/02/$ - see front matter © 2002 Published by Elsevier Science Ltd.
PII: S0967-0645(02)00056-5

1997). Large changes in heat distribution as a result of El Niños and La Niñas are communicated through Kelvin and Rossby waves from the equatorial region to higher latitudes along the west coasts of North and South America, and virtually throughout the world through changes in the atmospheric circulation (Philander, 1990). In spite of this accepted importance and the extensive scientific data set resulting from an enormous gathering effort by international JGOFS investigators, the chemical and biological functioning of this quasi-continuous upwelling system is not understood at the most basic level, that of control processes.

Well-known features of the system include low and relatively invariant phytoplankton biomass measured as chlorophyll (Walsh, 1976; Barber and Chavez, 1991; Barber et al., 1996), the presence of primary nutrient concentrations well-elevated above that of the central gyres, and high $pCO_2$ concentrations that normally result in a positive efflux of $CO_2$ to the atmosphere (Murray et al., 1995). Since physics, biology, and chemistry all have a role in establishing the existence and magnitude of the $CO_2$ flux, reliable models have been sought to allow prediction of the state and functioning of this system, which is recognized in modern terms as complex, i.e. requiring non-linear analyses and equations.

The equatorial upwelling system may be addressed in broad terms as a quasi-continuous culture system akin to a chemostat (Frost and Franzen, 1992) in which the ratio of flow to volume of growth medium sets the loss rate and hence the growth rate (Monod, 1950). Regulation in a chemostat is obtained by formulating the feed nutrient mix to assure that one nutrient is present at limiting concentrations relative to all others. However, the simple fluid dilution model when applied to the equatorial upwelling system yields very low growth rates and nutrient concentrations at variance with data from the real ocean where measured growth rates are high, on the order of $1\,day^{-1}$ (Cullen et al., 1992). Grazing has been invoked as the control on loss rates (e.g. Walsh, 1976; Landry et al., 1997), with the consequence that the system appears to be organized through the interaction between limiting nutrient control of fluxes and grazing control of loss and growth rates. Although grazing control of algal biomass and loss rate is now widely accepted and the presence of at least two size fractions of phytoplankton are now known (Chavez et al., 1996; Bidigare and Ondrusek, 1996; Iriarte and Fryxell, 1995), the question of limiting nutrient is still debated. Since silicon is required for diatom growth and is in relatively lower supply compared to nitrogen from upwelling source depths, $Si(OH)_4$ has been proposed (Dugdale and Goering, 1970; Ku et al., 1995; Dugdale and Wilkerson, 1998) as the system-limiting nutrient. Iron has been shown to enhance diatom accumulation in a series of experiments (Coale et al., 1996; Price et al., 1994; Sanderson et al., 1995) conducted outside the upwelling zone, where the supply of Fe is primarily by the atmospheric input of dust. In the equatorial upwelling area, Fe is supplied from source water along with $NO_3$, $Si(OH)_4$, and $PO_4$ (Johnson et al., 1997). Unfortunately, little is known of the distribution of Fe, its form and regeneration, or its effect on primary nutrient uptake kinetics, making it difficult to construct realistic Fe-based ecosystem models.

In this communication we describe the response of equatorial upwelling production to changes in silicate in a Si-limited one-dimensional model with ten compartments that includes two phytoplankton groups, meso- and micro-zooplankton, nitrogen separated into new and regenerated forms, and silicate. The slope of the photosynthesis vs. irradiance curve, $\alpha$, is set somewhat below maximal as an implicit Fe effect (Chai et al., 2002). We assume for these model runs that sufficient Fe is upwelled or regenerated in the euphotic zone to assure the value of $\alpha$ and allow macronutrient concentration and light to regulate specific growth and uptake rates of the phytoplankton and that $Si(OH)_4$ regeneration in the euphotic zone is negligible (see Chai et al., 2002). The model output is compared to equatorial field data, especially JGOFS EqPac data.

## 2. Description of the model

The one-dimensional model described in detail in Chai et al. (2002) evolved from a one-dimen-

sional nitrogen-based five-compartment model of the equatorial Pacific (Chai et al., 1996) modified to incorporate existing Si-limited models (Dugdale et al., 1995; Dugdale and Wilkerson, 1998). The model has ten compartments (Fig. 1) in which $NO_3$ and $Si(OH)_4$ are upwelled along with $CO_2$ driven by the physical model and followed with $NH_4$ as they are distributed amongst the biological and detrital compartments of the model. Carbon and nitrogen are tracked together. Two categories of phytoplankton, $<5$-μm diameter cells (S1, picoplankton) and $>5$-μm diameter cells (S2, diatoms), and two classes of zooplankton, micro- (Z1) and meso-zooplankton (Z2), comprise the biological portion of the model. The detrital portion is split into detrital N and Si. Export of N occurs as (a) direct sinking of phytoplankton, primarily the larger diatoms, (b) sinking of fecal pellets from mesozooplankton grazing, and as (c) contribution to higher trophic levels through the mesozooplankton (loss). Si exports are only from direct sinking of diatoms and fecal pellet production. These losses are balanced by the upwelling of $NO_3$ and $Si(OH)_4$. The model is typically initiated with source (120 m depth) nutrient concentrations ($Si(OH)_4 < NO_3$) at both higher and lower than Levitus et al. (1993) values averaged for 5°S–5°N, 90–180°W (''Wyrtki box'', Wyrtki, 1981) and run for 1000 simulated days. Heat balance is calculated to ensure the model equilibrates at expected surface temperatures.

Model ecosystem surface results, obtained using source $Si(OH)_4 = 7.5\,\mathrm{mmol\,m^{-3}}$ and $NO_3 = 12\,\mathrm{mmol\,m^{-3}}$ (Fig. 2) and defined as the ''standard run'', show the picoplankton (S1) to have the most active pathways for N, with a large proportion circulating as $NH_4$ ($\rho NH_4 = 0.151\,\mathrm{mmol\,N\,m^{-3}\,day^{-1}}$) and taking up more $NO_3$ than diatoms (S2), $0.044\,\mathrm{mmol\,N\,m^{-3}\,day^{-1}}$ vs. $0.032\,\mathrm{mmol\,N\,m^{-3}\,day^{-1}}$, respectively. The picoplankton constitute the major phytoplankton biomass, $0.178\,\mathrm{mmol\,N\,m^{-3}}$ vs. $0.089\,\mathrm{mmol\,N\,m^{-3}}$ for diatoms. The mesozooplankton biomass is about twice that of the microzooplankton, $0.585\,\mathrm{mmol\,N\,m^{-3}}$ vs. $0.351\,\mathrm{mmol\,N\,m^{-3}}$, although the microzooplankton process a larger proportion of the

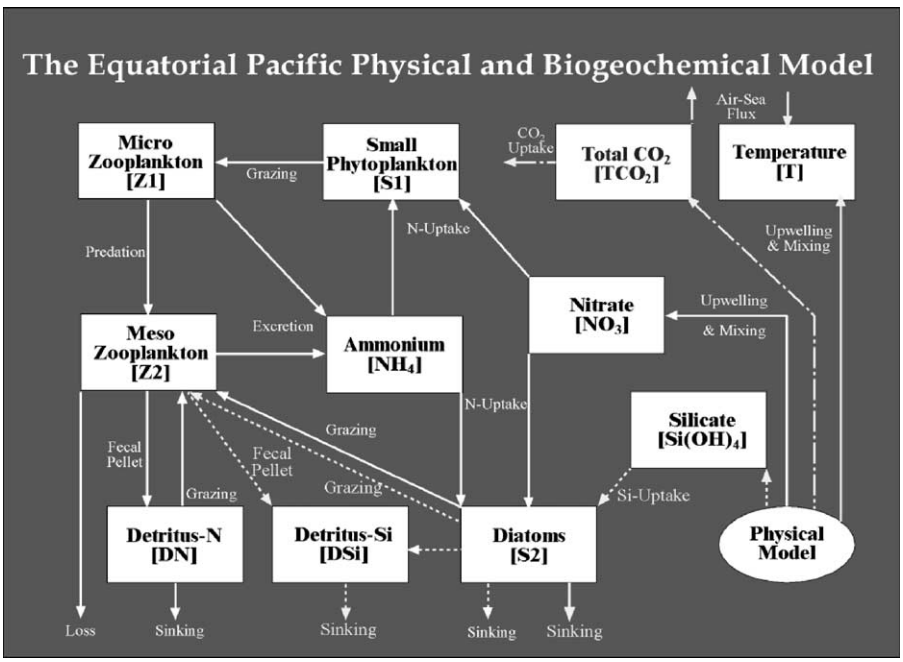


Fig. 1. The inter-compartmental flowchart of the one-dimensional model. The flow of nitrogen is indicated by solid line; the flow of silicon is indicated by dashed line; and the carbon flow is indicated by line–dashed line.

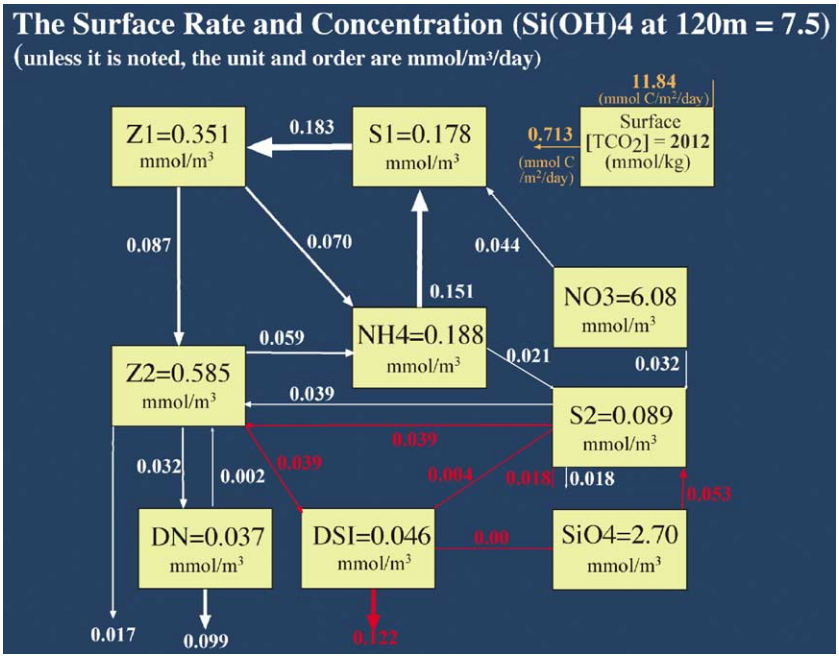


Fig. 2. One-dimensional model output generated using source $Si(OH)_4$ concentration (at 120 m depth) of 7.5 mmol $m^{-3}$ (''standard run''). White lines indicate N flow, red lines indicate silicon flow, and orange is flow of carbon.

circulating N and C, e.g. excretion rates are 0.070 mmol N $m^{-3}$ $day^{-1}$ vs. 0.059 mmol N $m^{-3}$ $day^{-1}$. Partitioning of $CO_2$ is shown separately in the upper right box of Fig. 2. Next, we describe the results of sensitivity experiments and comparison to JGOFS EqPac equatorial data from cruises in 1992 to the region of 140°W.

## 3. Sensitivity experiments

A series of experiments on model sensitivity to input parameters showed that model output was sensitive to a variety of parameters (Chai et al., 2002) including the maximum mesozooplankton grazing rate and to the regeneration rate of Si in the euphotic zone. Our interests here are primarily in the effect of changing source $Si(OH)_4$ concentration, and we describe a series of sensitivity experiments that were made to observe the details of Si limitation in the model.

Sensitivity of the model to changes in the source $[Si(OH)_4]$ at 120 m depth was examined (Table 1) by changing the concentration from a ''standard'' value, 7.5 to 12.5 mmol $m^{-3}$ (increase of +67%) and 3.0 mmol $m^{-3}$ (decrease of −60%). The $NO_3$ concentration at 120 m depth was held constant at 12.0 mmol $m^{-3}$. The ratio of diatom to picoplankton nitrogen biomass and nitrate and ammonium uptake, and the detrital Si/N ratio were strongly sensitive to changes in source $Si(OH)_4$ concentration. Surface $NO_3$ and $Si(OH)_4$ concentrations were most sensitive to reduced source $Si(OH)_4$ concentrations. Since a number of variables showed sensitivity to source $[Si(OH)_4]$, this analysis was expanded to evaluate the model response to a wider range of source $Si(OH)_4$ concentrations.

### 3.1. Model response of surface nutrients and biomass to a range of source $[Si(OH)_4]$

A series of model runs was made using seven different source $Si(OH)_4$ concentrations ranging from 3 to 15 mmol $m^{-3}$ (3, 5, 7.5, 8.75, 10, 12.5, and 15 mmol $m^{-3}$), corresponding to the full range of JGOFS equatorial values of 3–13 mmol $m^{-3}$

Table 1
Percentage changes in biomass and rate parameters produced by the one-dimensional model resulting from an increase or decrease in source-water $Si(OH)_4$ from the "standard run"

| Source $Si(OH)_4$, % change | Surface nutrients, % change | | | Surface PN ratio, % change | Surface uptake ratio, % change | | Detrital ratio, % change |
|---|---|---|---|---|---|---|---|
| | $NO_3$ | $Si(OH)_4$ | $NH_4$ | Diatom N:Picoplankton N | Diatom $\rho NO_3$:Picoplankton $\rho NO_3$ | Diatom $\rho NH_4$:Picoplankton $\rho NH_4$ | Detrital Si:N |
| −60 | −65 | −46 | −51 | −72 | −89 | −87 | −74 |
| +67 | +19 | +19 | +46 | +137 | +81 | +220 | +129 |

Table 2
Equatorial ranges of near-surface and source nutrient concentrations for comparison with one-dimensional model range

| Cruise | Location | Depth (m) | $Si(OH)_4$ (mmol $m^{-3}$) | | $NO_3$ (mmol $m^{-3}$) | |
|---|---|---|---|---|---|---|
| | | | Mean | Range ($n$) | Mean | Range ($n$) |
| TT007 | 0, 140°W | 10 | 2.22 | 1.98–2.33 ($n = 3$) | 2.93 | 2.86–3.04 ($n = 3$) |
| TT008 | 0, 140°W | 5 | 2.23 | 1.58–2.62 ($n = 12$) | 2.84 | 2.17–3.26 ($n = 12$) |
| TT011 | 0.24°N, 140°W | 3 | 2.48 | $n = 1$ | 6.07 | $n = 1$ |
| TT012 | 0, 140°W | 0 | 3.79 | 2.6–4.96 ($n = 19$) | 5.95 | 4.82–7.50 ($n = 19$) |
| Surface overall range | | | | 1.58–4.96 | | 2.17–7.50 |
| Modeled range | | | | 1.8–5.3 | | 2.4–6.0 |
| TT007 | 0, 140°W | 120 | 9.43 | 8.16–11.79 ($n = 3$) | 14.22 | 13.07–15.95 ($n = 3$) |
| TT008 | 0, 140°W | 120 | 6.57 | 3.33–11.16 ($n = 14$) | 11.71 | 7.66–15.88 ($n = 14$) |
| TT011 | 0.24°N, 140°W | 118 | 8.25 | $n = 1$ | 13.39 | $n = 1$ |
| TT012 | 0, 140°W | 120 | 9.96 | 6.11–13.08 ($n = 19$) | 12.74 | 10.47–14.32 ($n = 18$) |
| Source overall range | | | | 3.33–13.08 | | 7.66–15.95 |
| Modeled range | | | | 3.0–15.0 | | 12.0 |

(Table 2). Source $NO_3$ concentration was held at 12.0 mmol $m^{-3}$. Surface $[Si(OH)_4]$ showed a more or less linear increase over the full range of source $[Si(OH)_4]$, while surface $[NO_3]$ increased rapidly at the low source $[Si(OH)_4]$ reaching a maximum at 7.5 mmol $m^{-3}$, declining thereafter (Fig. 3a). The modeled surface $Si(OH)_4$ concentration varied only over the range 1.86–5.22 mmol $m^{-3}$. This is characteristic of this chemostat-like system, locking the surface $Si(OH)_4$ concentrations into a narrow range with a wide range of source $Si(OH)_4$ concentrations. This may be a useful diagnostic tool for comparison of model to field data. The biomass of S2, diatoms (Fig. 3b) increased at nearly linear rates with increasing source $[Si(OH)_4]$ while the picoplankton, S1, showed a rapid decrease in the 3–7.5 mmol $m^{-3}$ $[Si(OH)_4]$ range after which the population stabilized and remained constant (Fig. 3b). The microzooplankton biomass, Z1 remained virtually unchanged with changes in source $[Si(OH)_4]$ (Fig. 3c), while the mesozooplankton, Z2, increased linearly in similar

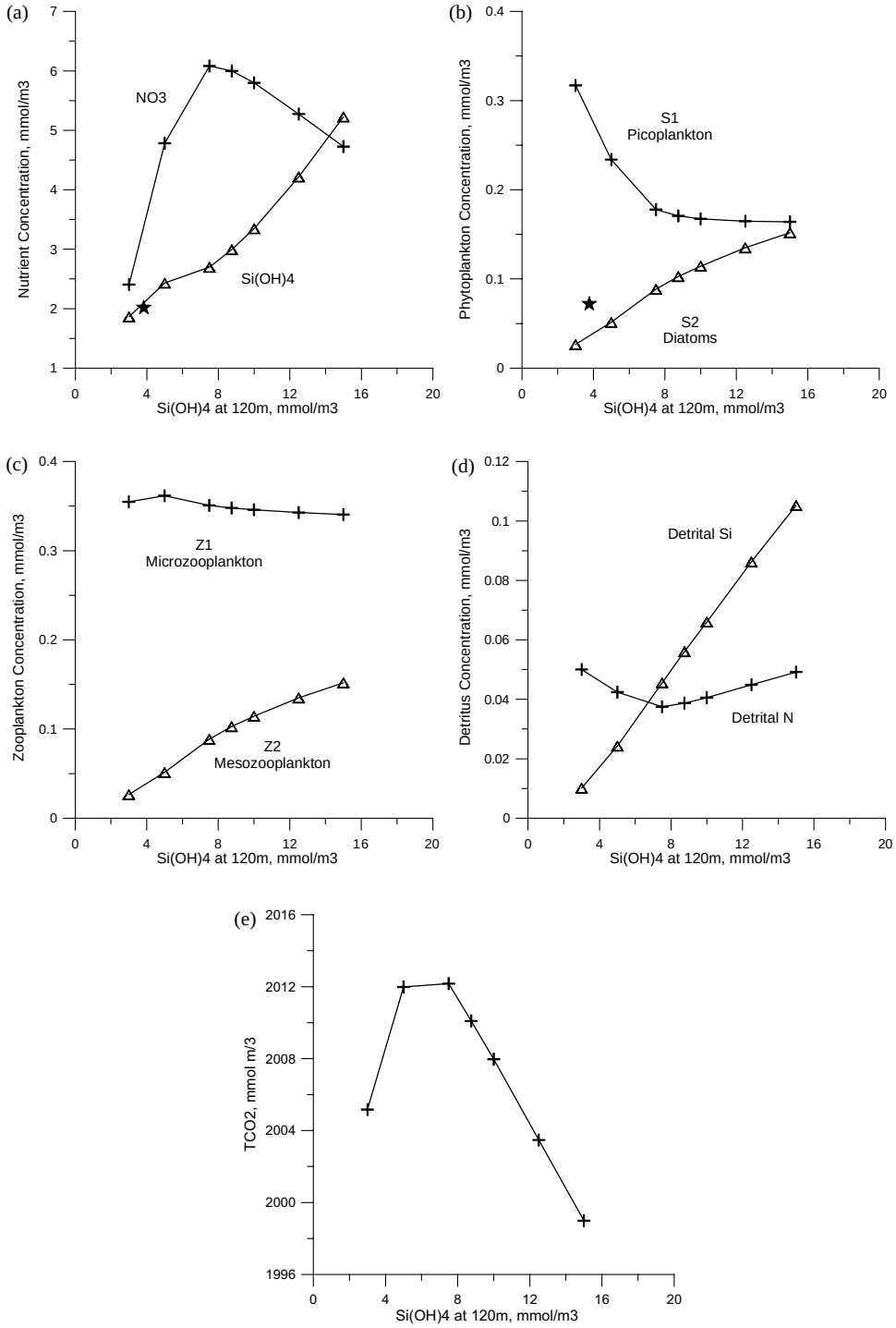


Fig. 3. Surface response of the one-dimensional model to changes in source $Si(OH)_4$ concentration, (a) nitrate and silicate concentrations, mmol $m^{-3}$, (b) picoplankton (S1) and diatom (S2) biomass, mmol $m^{-3}$, (c) micro- (Z1) and macro-zooplankton (Z2) biomass, mmol $m^{-3}$, (d) detrital N and Si, mmol $m^{-3}$, and (e) $TCO_2$, mmol $m^{-3}$. Asterisks are data from Leynaert et al. (2001).

fashion to the diatoms. Detrital N (Fig. 3d) showed only small changes, a decrease to a minimum at source $Si(OH)_4 = 7.5\,mmol\,m^{-3}$, while detrital Si showed a linear increase throughout the range of source concentrations. Surface $TCO_2$ initially increased (Fig. 3e) with increasing source $[Si(OH)_4]$. This is because with increasing source $[Si(OH)_4]$ the diatom population increases and outcompetes the picoplankton (Fig. 3b), and then the turndown in $NO_3$ and $TCO_2$ results due to the full dominance of the primary production by the diatoms. Diatoms control the nutrient conditions in the euphotic zone with high $NO_3$ and $CO_2$ uptake.

### 3.2. Model response of uptake and export to a range of source $[Si(OH)_4]$

Nitrate uptake ($\rho NO_3$, $mmol\,m^{-3}\,day^{-1}$), by the two phytoplankton fractions as a function of source $[Si(OH)_4]$ (Fig. 4a), followed a similar pattern to changes in biomass, i.e. a quasi-linear increase for the diatoms and a rapid initial decrease in uptake by the picoplankton. The entire phytoplankton community (S1 + S2) first showed a decrease, then leveled off, and finally increased. Ammonium uptake ($\rho NH_4$) showed a similar pattern for all fractions (S1, S2, and S1 + S2), a decrease and then leveling off at $7.5\,mmol\,m^{-3}$ source $Si(OH)_4$ (Fig. 4b). However, the rate of $NH_4$ uptake by the picoplankton was higher than for diatoms. The combination of decreased total N uptake by picoplankton and the linear increase in N uptake by the diatoms results in a minimum total uptake for the entire phytoplankton at $7.5\,mmol\,m^{-3}$ source $Si(OH)_4$ (Fig. 4c).

The $f$-ratios (proportion new production calculated as $\rho NO_3$/total $\rho N$) for the two phytoplankton size fractions and for the total phytoplankton community (Fig. 4d) showed higher values for the diatoms than for the picoplankton by a factor of about 3, indicating the predominately regenerative productivity of the picoplankton and the predominately new production mode of the diatoms. The range of overall surface community $f$-ratio was very small, about 0.3–0.4. The proportion of new production carried out by diatoms (Fig. 4e), increases quasi-linearly from $<0.1$ at the lowest $Si(OH)_4$ source concentration to nearly 0.8 at the highest; the curve is steepest up to the mid-range and tends to level off thereafter.

The biomass specific $NO_3$ uptake rates, $VNO_3$ ($day^{-1}$) representative of growth rates, vs. changing source $[Si(OH)_4]$ (Fig. 4f) showed a slight increase by the diatom fraction and a relatively small decrease in the picoplankton rate. The specific $NH_4$ uptake rates ($VNH_4$) (Fig. 4g) initially increased for both phytoplankton fractions with increasing source $[Si(OH)_4]$ and then leveled off.

The integrated export production of N and Si at 120 m (Fig. 4h) as a function of $[Si(OH)_4]$ at 120 m showed N export to decrease to a minimum at $7.5\,mmol\,m^{-3}$ source Si(OH) and to increase thereafter. Modeled Si export increases almost linearly from initial low values of about 0.35–$3.2\,mmol\,m^{-2}\,day^{-1}$. The downturn in N export is due to increased mesozooplankton grazing on picoplankton and then the increase in N export occurs as diatom production and mesozooplankton grazing on diatoms becomes the dominant export mechanism.

### 3.3. Internal control mechanisms of the model in response to a range of source $[Si(OH)_4]$

The model was designed as a chemostat-like system in which the diatoms are limited by $Si(OH)_4$ and diatom growth rate is set by the loss rates, primarily grazing. If the model is actually functioning in this manner, it should be possible to retrieve the kinetics for $Si(OH)_4$ uptake (i.e. uptake by diatoms) for comparison with the Michaelis–Menten parameters that were used as model inputs. Source $[Si(OH)_4]$ was varied from 3 to $15\,mmol\,m^{-3}$, and the modeled output of surface $[Si(OH)_4]$ (Fig. 3a) and Si uptake was used to evaluate the kinetics and Michaelis–Menten parameters. Modeled specific diatom growth rate $VSi$, (i.e. $\rho Si$ divided by biomass expressed as biogenic silica) showed a hyperbolic response to modeled surface $[Si(OH)_4]$ (Fig. 5a). When transformed to a linear Woolf plot ($V$ vs. $V/S$), which would reveal any non-Michaelis trend in the data (Fig. 5b), it is apparent that model data conform to the Michaelis–Menten equation. Michaelis–Menten

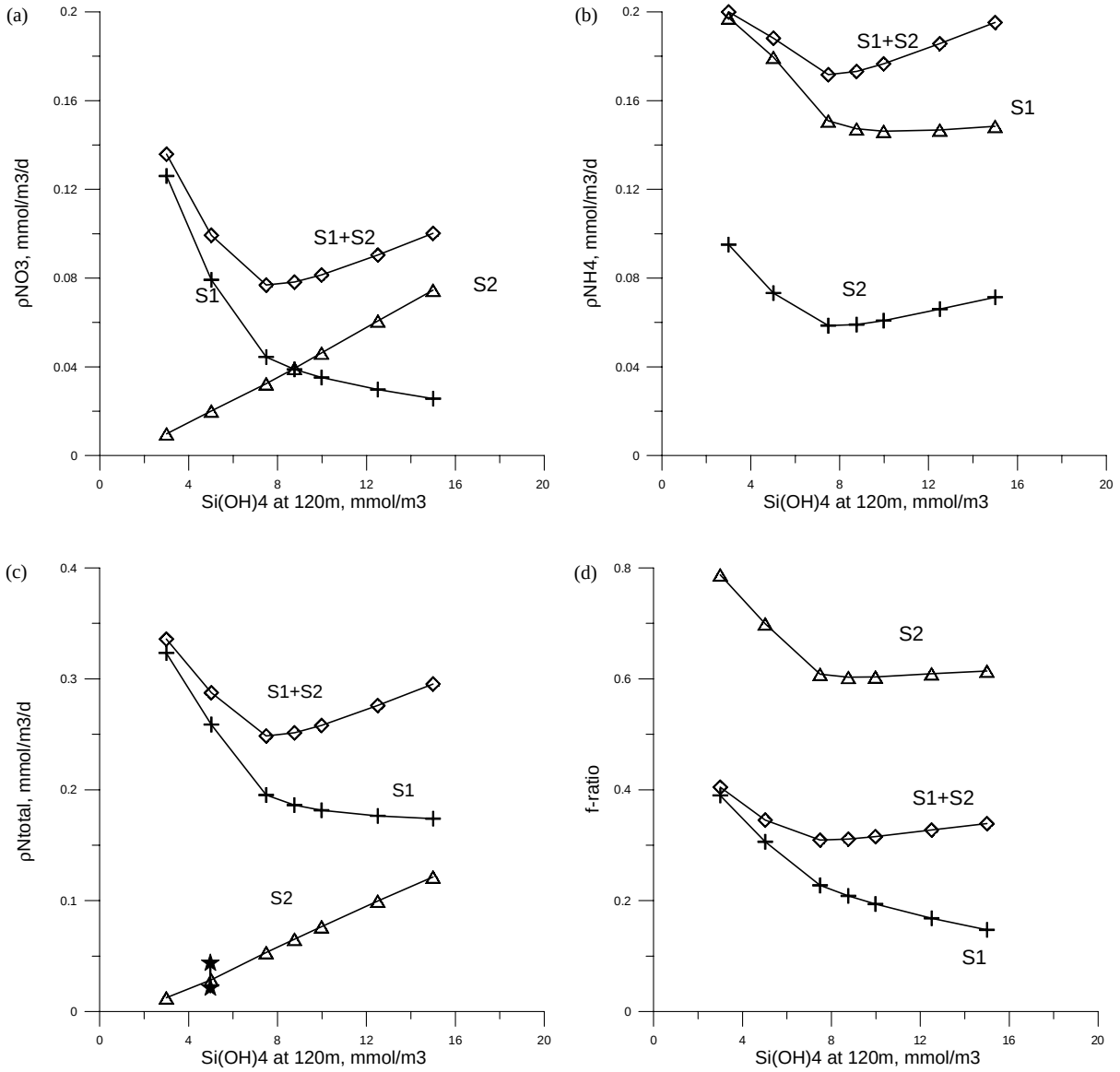


Fig. 4. Surface response of picoplankton (S1), diatoms (S2) and total phytoplankton (S1 + S2), in the one-dimensional model to changes in source $Si(OH)_4$ concentration, (a) $\rho NO_3$, mmol m$^{-3}$ day$^{-1}$, (b) $\rho NH_4$, mmol m$^{-3}$ day$^{-1}$, (c) $\rho N_{total}$, mmol m$^{-3}$ day$^{-1}$, (d) $f$-ratio, (e) proportion of $\rho NO_3$ by diatoms to total $\rho NO_3$, (f) $VNO_3$, day$^{-1}$, (g) $VNH_4$, day$^{-1}$, and (h) integrated export production of N and Si, mmol m$^{-2}$ day$^{-1}$. Stars are data range from Leynaert et al. (2001).

parameters of $K_S = 2.97\,\text{mmol}\,\text{m}^{-3}$ and a $V_{max}$ of $1.26\,\text{day}^{-1}$ that were retrieved from the model after 1000 days compare well with the values used as inputs for the model ($K_S = 3.0\,\text{mmol}\,\text{m}^{-3}$ and $V_{max} = 1.5\,\text{day}^{-1}$, equivalent to a growth rate of $3\,\text{day}^{-1}$ with 24 h of light). The model behaves as a chemostat-like system, with the nutrient source composition assuring $Si(OH)_4$ limitation, and the loss rates setting the surface $Si(OH)_4$ concentrations. The first kinetics for $Si(OH)_4$ uptake obtained at the equator, 180°W (Leynaert et al., 2001), $K_{Si(OH)4} = 2.42\,\text{mmol}\,\text{m}^{-3}$, $V_{max} = 1.25\,\text{day}^{-1}$

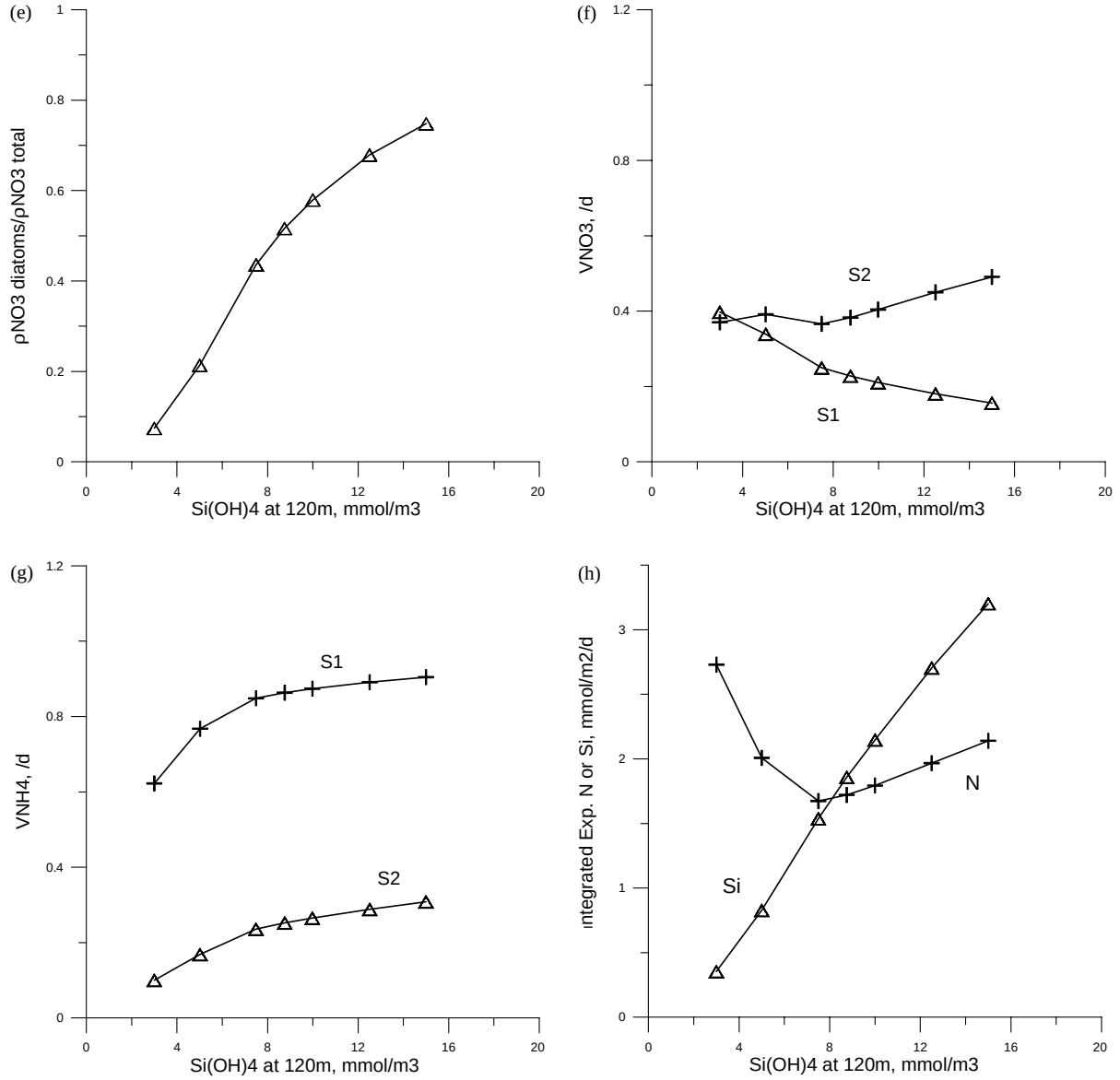


Fig. 4 (*continued*).

are in good agreement with the $Si(OH)_4$ kinetics used in the one-dimensional model.

To test whether the specific growth rates of the diatoms are set by the loss rates in terms of grazing, the modeled output of $V$Si ($= V\mathrm{N}_{\mathrm{total}} =$ growth rate) was plotted as a function of the modeled mesozooplankton grazing rate (Fig. 6a) and showed a linear response to support this. A similar analysis for the picoplankton (Fig. 6b) using the model output values for $V\mathrm{N}_{\mathrm{total}}$ by the picoplankton and grazing by the microzooplankton showed a similar positively linear relationship. Grazing rate is controlling most phytoplankton growth rates.

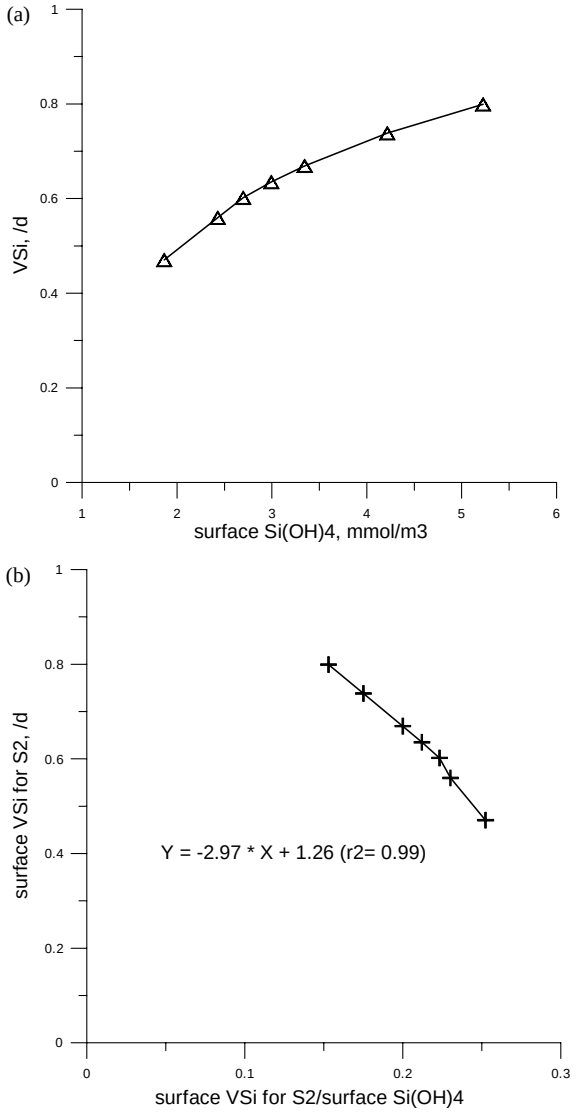


Fig. 5. Surface response of (a) silicate uptake, $V$Si vs. surface $Si(OH)_4$ concentration from the one-dimensional model, with fitted Michaelis–Menten hyperbola using $K_{Si(OH)4} = 3.0$ and $V_{max} = 0.7\,day^{-1}$ and (b) Woolf plot ($V$ vs. $V/S$) for data in (a).

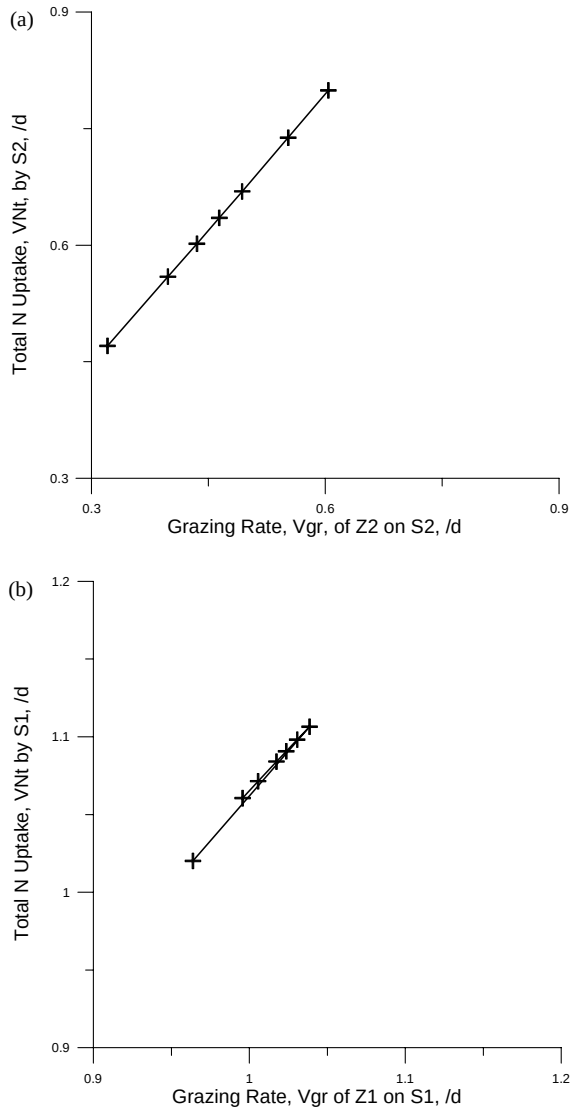


Fig. 6. Surface response of one-dimensional model of (a) total nitrogen uptake, $V\mathrm{N}_{total}$, by diatoms (S2) vs. macrograzing rate of Z2 on S2 and (b) total nitrogen uptake, $V\mathrm{N}_{total}$, by picoplankton (S1) vs. micrograzing rate of Z1 on S1.

### 3.4. Model response of nutrients and $TCO_2$ at depth, to a range of source [$Si(OH)_4$]

For four different source $[Si(OH)_4]$, 3.0, 5.0, 7.5, and 12.5 mmol $m^{-3}$, the model output for $NO_3$ and $Si(OH)_4$ at depths ranging from 0 to 200 m shows the drawdown of these nutrients (Fig. 7). The slope of the $Si(OH)_4$:$NO_3$ disappearance varies directly as the source $[Si(OH)_4]$. Breakpoints occur in all four curves at 120 m depth and are due to the model procedure in which the initial nutrient conditions between 120 and 200 m are restored at every step in the computation. Between 0 and 120 m all variables are allowed to vary. These breakpoints also appear in field data from JGOFS

(Dugdale and Wilkerson, 1998) and in nature are the result of biologically and physically dominated processes in the upper water column and deep-source water regeneration effects below the euphotic zone.

When the same procedure was carried out for $TCO_2$ vs. $Si(OH)_4$, the same breakpoints occurred around 120 m depth in the model output, again caused by the model procedure. The slope of $TCO_2$:$Si(OH)_4$ values from 0 to 200 m (Fig. 8a) increased with decreasing source $[Si(OH)_4]$ whereas the $TCO_2$:$NO_3$ disappearance slopes increased with increasing source $[Si(OH)_4]$ (Fig. 8b). At 120 m depth, $NO_3$ is held at 12 mmol $m^{-3}$ and values are progressively interpolated to match the $NO_3$ vs. depth slope of Levitus et al. (1993). Slopes for $TCO_2$:$NO_3$ are lower than $TCO_2$:$Si(OH)_4$ due to the regeneration of nitrogen through grazing.

## 4. Comparison of model results with field data

### 4.1. Mean nutrient concentrations

A variety of field data collected in the equatorial Pacific was used to compare with model input and output values. The JGOFS EqPac data used for comparison with model output was obtained during cruises that experienced a wide range of oceanic conditions. TT007 and TT011 were survey cruises that made sections across 140°W, whereas TT008 and TT012 were time-series cruises that sampled intensely only at the equator. TT007 was conducted during Spring 1992 during a strong El Niño (Kessler and McPhaden, 1995). Means of source-depth nutrient concentrations (Table 2)

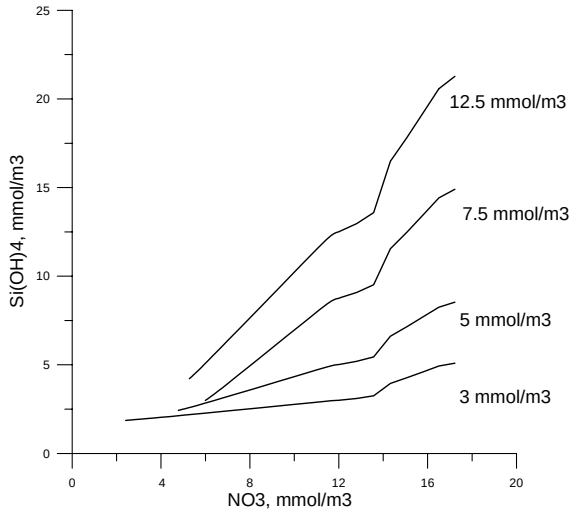


Fig. 7. $Si(OH)_4$ vs. $NO_3$ concentration from surface to 200 m, modeled drawdown in response to different source $Si(OH)_4$ concentrations (3, 5, 7.5, and 12.5 mmol $m^{-3}$ $Si(OH)_4$).

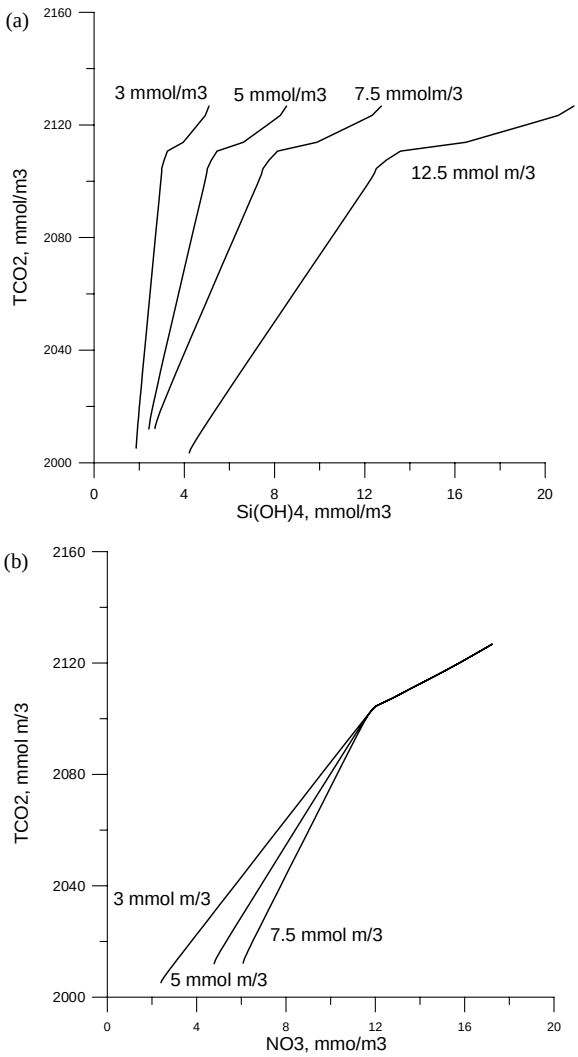


Fig. 8. $TCO_2$ vs. (a) $[Si(OH)_4]$ and (b) $[NO_3]$ from surface to 200 m, modeled drawdown in response to different source $Si(OH)_4$ concentrations (3, 5, 7.5, and 12.5 mmol $m^{-3}$ $Si(OH)_4$).

show consistently lower values for $[Si(OH)_4]$ than $[NO_3]$, by about 3–5 mmol m$^{-3}$. The range of source $[Si(OH)_4]$, 3.33–13.08 mmol m$^{-3}$, corresponds almost exactly to the range of source values used in the model experiments (3–15 mmol m$^{-3}$). The model source $[NO_3]$ of 12 mmol m$^{-3}$ lies at about the mid-point of the observed source $[NO_3] = 11.8$ mmol m$^{-3}$. Mean near-surface $[Si(OH)_4]$ measured during JGOFS was less than $[NO_3]$ and showed less variation than $[NO_3]$. The near-surface nutrient field data ranges compare very closely with the modeled output values. At 0°, 180°W, where Leynaert et al. (2001) made $^{32}$Si measurements of $Si(OH)_4$ uptake, the $Si(OH)_4$ source concentration was about 4.0 mmol m$^{-3}$. The surface $Si(OH)_4$ concentration was about 2 mmol m$^{-3}$ (their Fig. 2b) and when plotted in Fig. 3a shows good agreement with one-dimensional model simulations.

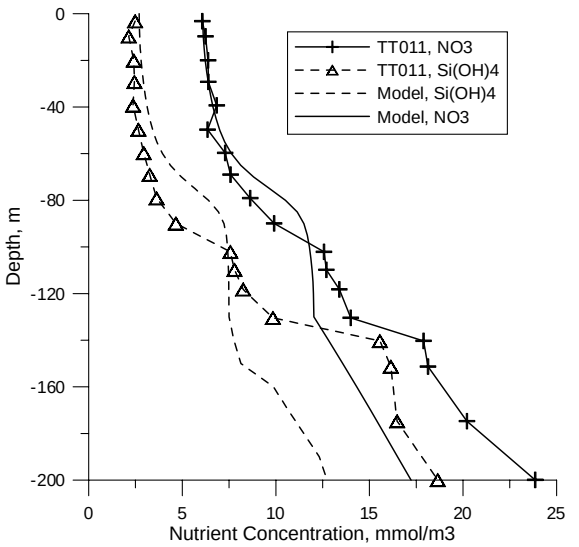


Fig. 9. Comparison of nitrate and silicate concentrations from one-dimensional model and JGOFS TT011 data from 0.25°N.

### 4.2. Nutrient concentrations and $Si(OH)_4$ uptake vs. depth

The modeled vertical distribution of $NO_3$ and $Si(OH)_4$ from 0 to 200 m obtained using a source $[(Si(OH)_4] = 7.5$ mmol m$^{-3}$ and from JGOFS data at 0.25°N, 140°W from TT011 (fall 1992 cruise) show the model and data to be in good agreement, both for shape and concentrations down to about 120 m (Fig. 9), the boundary below which model values are held constant. The model reproduces well the characteristic of the equatorial Pacific, non-limiting concentrations of $NO_3$ and lower levels of $Si(OH)_4$ in the euphotic zone (upper 120 m) due to biological activity. Modeled uptake of $Si(OH)_4$ with depth shows a pattern similar to that of photosynthesis and in good agreement with the vertical profile of $Si(OH)_4$ uptake (Fig. 10) obtained by Leynaert et al. (2001) using $^{32}$Si, at 0°, 180°W, except for surface inhibition. This term is not considered in the present one-dimensional model.

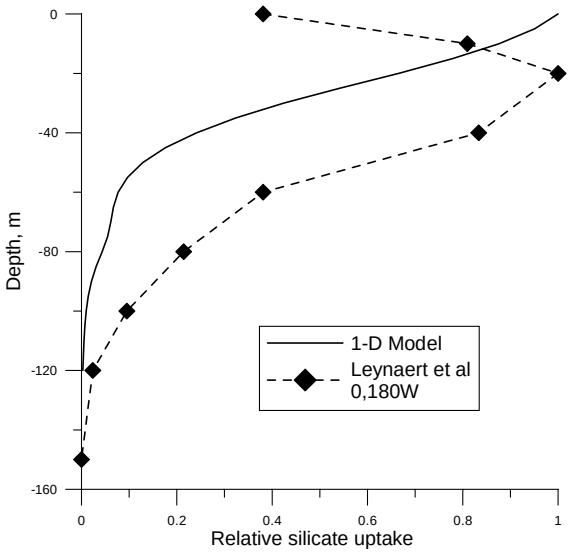


Fig. 10. Comparison of silicate uptake from one-dimensional Model and field data from 0, 180°W (Leynaert et al., 2001).

### 4.3. Biomass concentrations

The concentrations and proportions of the two size fractions produced by the one-dimensional model cannot be compared with JGOFS data since no such measurements were made on these cruises. However, Peña et al. (1990) made fractionated chlorophyll measurements along 135°W from 15°N to 15°S in 1988. From their Fig. 5 the

percentages of large (>1 μm) and small (<1 μm) chlorophyll fractions can be estimated as 60% and 40%. From our Fig. 3b the source $Si(OH)_4$ to support a nearly 1:1 biomass ratio is 15 mmol $m^{-3}$, about the concentration observed by Peña et al. (1990; their Fig. 1). Modeled phytoplankton biomass also can be compared with data from Chavez et al. (1991). Converting their carbon biomass values to nitrogen and lumping picoplankton and autotrophic flagellates together gives a value of 0.20 mmol N $m^{-3}$ for "small" phytoplankton and 0.088 mmol N $m^{-3}$ for diatoms. Plotting the point for diatom biomass on Fig. 3b corresponds to a source $Si(OH)_4 = 7.5$ mmol $m^{-3}$. Iriarte and Fryxell (1995) reported a maximum biomass concentration of 0.077 mmol N $m^{-3}$ (converted from their carbon values) in the microphytoplankton during the passage of the instability wave during JGOFS TT012 fall time-series cruise. This elevated biomass concentration corresponded to a large increase in diatoms. The one-dimensional model source $Si(OH)_4$ necessary to support this diatom population is about 6.5 mmol $m^{-3}$ (Fig. 3b). The $Si(OH)_4$ source concentrations predicted by the one-dimensional model from the diatom biomass field data fall close to the "standard run" source concentration, 7.5 mmol $m^{-3}$, and close to the mean $Si(OH)_4$ concentration at 120 m depth for TT011 and TT012, 8.25 and 9.96 mmol $m^{-3}$, respectively. The one-dimensional model predictions of fractionated phytoplankton biomass are consistent with the few available field observations. The range of diatom concentrations calculated from biogenic silica measurements, observed by Leynaert et al. (2001) at low $Si(OH)_4$ source concentration, are in good agreement with the one-dimensional model simulation (Fig. 3b); low $Si(OH)_4$ source concentration is correlated with low surface diatom concentrations (i.e. biogenic silica values).

### 4.4. Nutrient uptake rates

Mean new and regenerated N production ($\rho NO_3$ and $\rho NH_4$) and the ratio of new to total N production, $f$-ratio, measured in field studies are compared with the one-dimensional model results (Table 3). The modeled $\rho NO_3$ output using three source $[Si(OH)_4]$ compares well with field data except for cruise TT007 where the field data are lower by about 50%; this study took place during the 1992 El Niño. The $\rho NH_4$ model output values compare well with cruise data except for TT011 and FLUPAC when the observed data are higher by about 50%. The modeled $f$-ratios compare well with TT008 and TT012 but are higher than the other field observations. The field $\rho NH_4$ values vary most from the modeled data, e.g. TT011 $\rho NH_4$ values are twice modeled values, forcing the field measured $f$-ratios to low values. The TT007 measurements made during El Niño conditions with non-existent upwelling conditions (for which the one-dimensional model is not designed) have low $f$-ratio values due to low $\rho NO_3$ values. Direct measurements of $Si(OH)_4$ uptake using the tracer $^{32}Si$ (Leynaert et al., 2001) were converted to N and plotted with the one-dimensional model results in (Fig. 4c). These uptake rates, observed at low $Si(OH)_4$ source concentrations, agree well with the one-dimensional model predictions of low uptake rates under low $Si(OH)_4$ supply conditions. A comparison of both surface and depth integrated $Si(OH)_4$ uptake rates and diatom biomass from Leynaert et al. (2001) and Blain et al. (1997) show the modeled data ranges to match the field values (Table 4).

### 4.5. Export rates

Field measurements of N, Si, and C flux from shallow sediment traps are sparse, but the few available are compared with the one-dimensional model in Table 5. The modeled values compare well with the TT011 data, but are higher than the TT007 data, as would be expected from similar results for data and modeled $\rho NO_3$ comparisons in Table 3. Mean modeled N export, 0.85 mmol $m^{-2}$ $day^{-1}$, is close to the mean measured N export values from both JGOFS and OLIPAC cruises. The range of modeled N export values, 0.69–0.98 mmol $m^{-2}$ $day^{-1}$ lies within the measured range of estimates for TT011 in the 2°N–2°S region. The one-dimensional-model values for Si export for the "standard run" (7.5 mmol $m^{-3}$ source $Si(OH)_4$) compares well with the TT011 data. The Si export calculated using the

Table 3
Equatorial nutrient uptake rates measured during JGOFS EqPac and other cruises for comparison with one-dimensional model output

| | | $\rho NO_3$ (mmol m$^{-2}$ day$^{-1}$) | $\rho NH_4$ (mmol m$^2$ day$^{-1}$) | $\rho N_{Total}$ (mmol m$^2$ day$^{-1}$) | $f$-ratio | Reference |
|---|---|---|---|---|---|---|
| One-dimensional model | | | | | | |
| Source $Si(OH)_4 = 3$ | | 3.25 | 8.93 | 12.18 | 0.27 | |
| Source $Si(OH)_4 = 7.5$ | | 1.96 | 6.80 | 8.76 | 0.22 | |
| Source $Si(OH)_4 = 15$ | | 2.45 | 7.30 | 9.75 | 0.25 | |
| JGOFS EQPAC | | | | | | |
| TT007 | 2°N–2°S, 140°W | 0.72 | 5.82 | 6.54 | 0.11 | McCarthy et al. (1996) |
| TT007 | 0, 140°W | 0.48 | 6.81 | 7.29 | 0.07 | McCarthy et al. (1996) |
| TT008 | 0, 140°W | 2.86 | 7.78 | 10.64 | 0.26 | Wheeler, JGOFS Web |
| TT011 | 2°N–2°S, 140°W | 2.80 | 17.45 | 20.25 | 0.13 | McCarthy et al. (1996) |
| TT011 | 0, 140°W | 2.60 | 15.36 | 17.97 | 0.14 | McCarthy et al. (1996) |
| TT012 | 0, 140°W | 3.32 | 8.92 | 12.20 | 0.27 | JGOFS Web |
| Other cruises | | | | | | |
| WEC 88 | 0, 150°W | 1.42 | 7.00 | 8.42 | 0.17 | Dugdale et al. (1992) |
| FLUPAC | 0, 150°W | 2.90 | 13.40 | 16.30 | 0.18 | Rodier and Le Borgne (1997) |
| OLIPAC | 0, 150°W | 1.87 | 12.54 | 14.41 | 0.13 | Raimbault et al. (1999) |

Table 4
Comparison of one-dimensional model results with published field data

| | Biogenic silica | $\rho$Si |
|---|---|---|
| | (mmol m$^{-3}$) | (mmol m$^{-3}$ day$^{-1}$) |
| Surface | | |
| One-dimensional model | 0.03–0.15 | 0.01–0.15 |
| Leynaert et al. (2001) | 0.65–0.70 | 0.02–0.04 |
| Blain et al. (1997) | 0.08 | |
| | (mmol m$^{-2}$) | (mmol m$^{-2}$ day$^{-1}$) |
| Integrated | | |
| One-dimensional model | 1.5–7.4 | 0.4–3.3 |
| Leynaert et al. (2001) | 7.4–9.5 | 2.1–2.9 |
| Blain et al. (1997) | | 2.0 |

lowest source $[Si(OH)_4]$, 3 mmol m$^{-3}$ is slightly higher than the lower TT007 flux estimates. Carbon export rates compare favorably between data and model output.

### 4.6. Response of surface nutrients to changes in source nutrient concentrations

The passage of an instability wave during the JGOFS TT012 cruise (Foley et al., 1997; Barber et al., 1996) gave a natural experiment of how the surface nutrients might respond to changes in source nutrients for comparison with the sensitivity experiments carried out with the one-dimensional model. $Si(OH)_4$ increased dramatically at 120 m from a minimum of 6 mmol m$^{-3}$ in early October to a maximum of 13 mmol m$^{-3}$ by October 16, 1992 (Fig. 11a, 2 weeks later). Large increases in diatoms were observed during this event (Iriarte and Fryxell, 1995). The excursions in source $Si(OH)_4$ concentration during this period were greater than those of $NO_3$, which varied from a low of 10 to a maximum of about 14 mmol m$^{-3}$ during the same time period. The one-dimensional

Table 5
Comparison of modeled vs. field data of export rates (mmol $m^{-2}$ $day^{-1}$) integrated to 120 m depth

| | Location | N export | Si export | C export | Reference |
|---|---|---|---|---|---|
| One-dimensional model | Wyrtki Box | | | | |
| Source $Si(OH)_4 = 3$ | | 0.69 | 0.35 | 5.04 | |
| Source $Si(OH)_4 = 7.5$ | | 0.88 | 1.54 | 6.42 | |
| Source $Si(OH)_4 = 15$ | | 0.98 | 3.20 | 7.15 | |
| Mean (*n*) | | 0.85 (3) | 1.70 (3) | 6.20 (3) | |
| Range | | 0.69–0.98 | 0.35–3.20 | 5.04–7.15 | |
| JGOFS EQPAC | | | | | |
| Mean (*n*) | | | | | Dunne et al. (1999, Fig. 4) |
| Range | | | | | Murray et al. (1996, Table 5) |
| TT007 | 2°N–2°S, | 0.53 (4) | 0.08 (2) | 4.1 (5) | |
| | 140°W | 0.38–0.95 | 0.05–0.1 | 2.3–6.3 | |
| TT007 | 0, 140°W | nd | nd | 6.1 | |
| TT011 | 2°N–2°S, | 1.87 (5) | 1.94 (5) | 11.8 (4) | |
| | 140°W | 0.6–4.65 | 0.4–3.9 | 3.6–19.5 | |
| TT011 | 0, 140°W | 1.3 | 1.4 | 10 | |
| OLIPAC (mean) | 0, 150°W | 0.68 | | 7.1 | Dunne et al. (1999, Fig. 4) |

Conversion to C is N export multiplied by 7.3 (Chai et al., 2002).

model predicts that these changes in source [$Si(OH)_4$] would result in increased surface $Si(OH)_4$ and increased $NO_3$ until a certain concentration after which $NO_3$ would decrease (Fig. 3a). The changes in surface concentrations (Fig. 11b) are in accordance with model predictions; $NO_3$ increased markedly and then decreased. However, surface $Si(OH)_4$ concentration did not increase but remained nearly constant at about 4 mmol $m^{-3}$.

### 4.7. Drawdown in concentrations of $TCO_2$ vs. $Si(OH)_4$ and $NO_3$, 0–400 m

The slopes of $TCO_2$:$Si(OH)_4$ and $TCO_2$:$NO_3$ disappearance for TT011 (JGOFS fall 1992 cruise), 1°N–1°S, 140°W, 0–400 m presented in Dugdale and Wilkerson (1998) were compared with modeled slopes for 0–200 m (Fig. 8a and b), which show breakpoints in the data. The field data (to 400 m depth) (Dugdale and Wilkerson, 1998, their Fig. 1) show similar breakpoints, probably reflecting the relatively constant source water in the undercurrent and the modification of the water characteristics by physical and biological effects in the shallower waters.

### 4.8. $Si(OH)_4$ vs. $NO_3$ relationships with JGOFS data

The slopes and intercepts of the linear relationships between $Si(OH)_4$ vs. $NO_3$ (0–120 m) from modeled output obtained using seven different source [$Si(OH)_4$] compare well with slopes and intercepts from a variety of cruises to 2°N–2°S, 165°E–81°W (Fig. 12) summarized by Dunne et al. (1999; their Table 1). The model output gives a reversed J-shaped curve, composed of a downward slope where the field data fit well, and an upward curve at high slopes (= high source $Si(OH)_4$) due to $Si(OH)_4 > NO_3$ at 120 m in the model. The downward slope indicates the shallower slopes with positive intercepts (i.e. there is $Si(OH)_4$ when $NO_3 = 0$), implying incipient N limitation due to the small biomass of diatoms and the dominance of the picoplankton. In the model this occurs with low source [$Si(OH)_4$]. A negative intercept condition (Fig. 12) occurs with steeper $Si(OH)_4$ vs. $NO_3$ slopes (Fig. 7) when there is positive $NO_3$ when $Si(OH)_4 = 0$ as a consequence of the increased diatom biomass. This occurs in the model with source [$Si(OH)_4$] above 7.5 mmol $m^{-3}$.

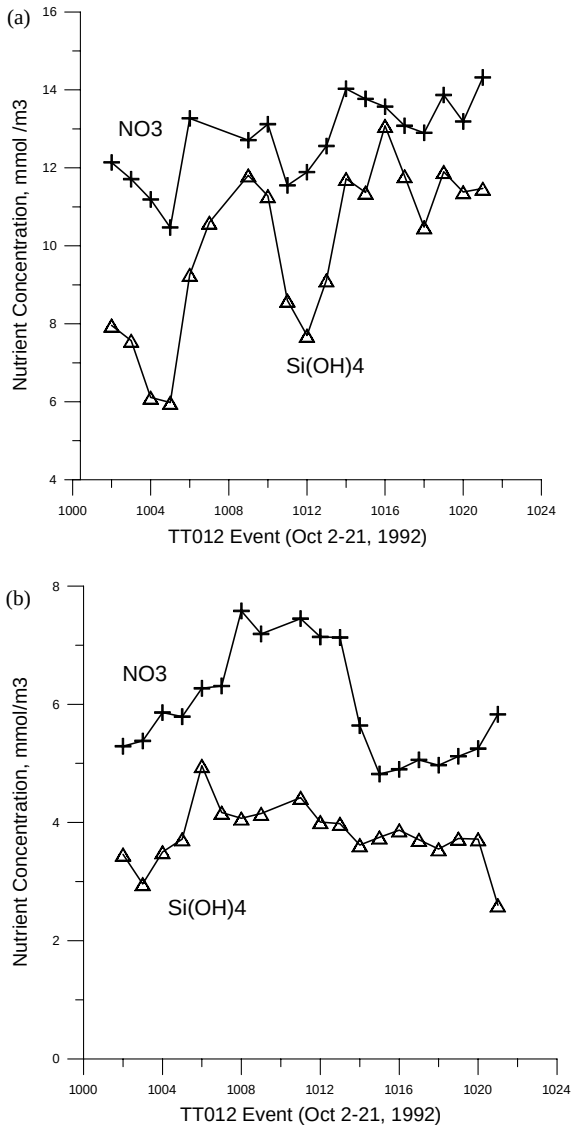


Fig. 11. $NO_3$ and $Si(OH)_4$ concentrations, mmol $m^{-3}$ at (a) 120 m depth and (b) surface, measured from October 2–21, JGOFS TT012 Time-Series Cruise.

Dugdale and Wilkerson (1998) plotted TT011 1°N–1°S, 140°W $Si(OH)_4$ vs. $NO_3$ for the upper 200 m and interpreted the slope of 1 to imply that all $NO_3$ was taken up by diatoms. Their model was subsequently constructed with all $NO_3$ uptake by diatoms and all $NH_4$ uptake by the picoplankton, a somewhat troublesome procedure in view of the known ability of picoplankton to utilize $NO_3$. The

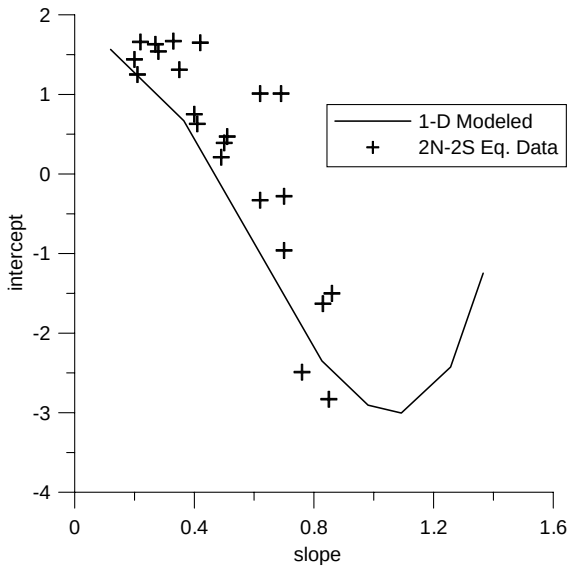


Fig. 12. Intercept vs. slopes from $NO_3$ vs. $Si(OH)_4$ relationships at 2°N–2°S, from Dunne et al. (1999), overlain with one-dimensional modeled data.

one-dimensional model provides a possible resolution to this apparent paradox. The $Si(OH)_4$:$NO_3$ slope for source $Si(OH)_4 = 8.75$ mmol $m^{-3}$ (Fig. 7) is 0.98, virtually identical to the TT011 data. At that concentration, $NO_3$ uptake is equally divided between diatoms and picoplankton (Fig. 4a).

The detrital Si:N ratios from sediment traps for equatorial cruises compiled by Dunne et al. (1999; their Table 3), plotted against mean slope of the $Si(OH)_4$:$NO_3$ in the upper 120 m for each cruise is compared with modeled (Fig. 13) detrital Si:N ratio and predicted slope of $Si(OH)_4$:$NO_3$ using seven source [$Si(OH)_4$]. The model agrees well with the JGOFS TT007 and TT011 data. The Zonal Flux and FLUPAC data that do not agree so well, were taken mostly in the western equatorial Pacific and fall in the low $Si(OH)_4$ vs. $NO_3$ slope, low detrital Si:N area of the figure. These low-slope data correspond to the positive intercept area in Fig. 12, with incipient N limitation.

### 4.9. Surface $TCO_2$ data

Field data of surface $TCO_2$ from 2°N to 2°S, 140°W (JGOFS TT011) show a decrease with

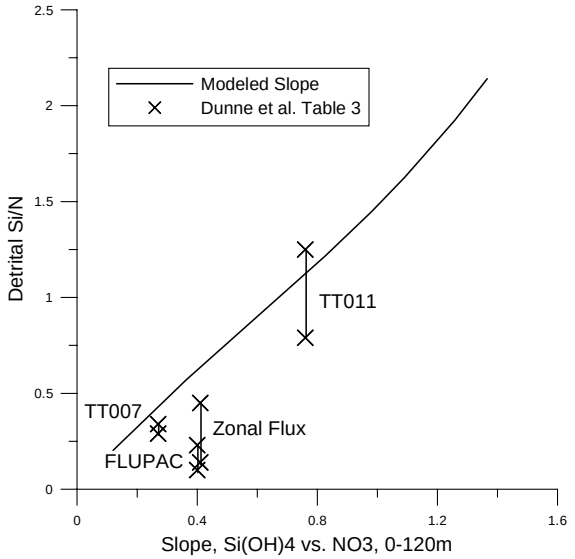


Fig. 13. Ratio of detrital Si:detrital N vs. slope of the $Si(OH)_4$ vs. $NO_3$ relationships for equatorial data from Dunne et al. (1999) compared to one-dimensional modeled ratio.

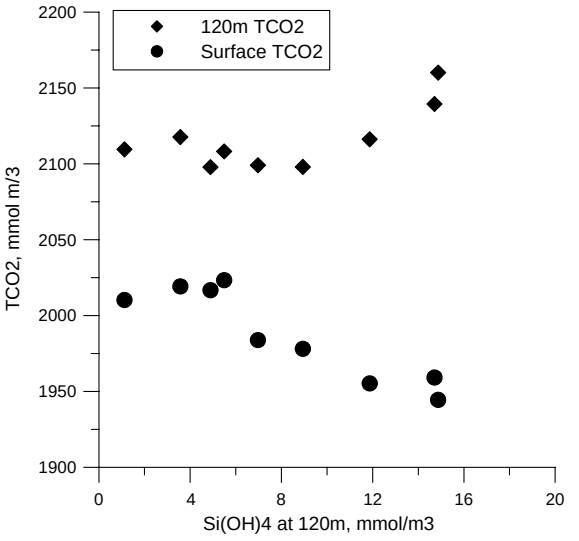


Fig. 14. $TCO_2$, mmol $m^{-3}$ at the surface and 120 m depth vs. $[Si(OH)_4]$ at 120 m depth measured during JGOFS TT011, 2°N–2°S, 140°W.

increasing source $[Si(OH)_4]$ at 120 m depth, above 5 mmol $m^{-3}$ (Fig. 14), and this pattern is consistent with the one-dimensional model results (Fig. 3e). The decreasing surface $TCO_2$ concentrations are a result of processing in the euphotic zone since the 120 m $TCO_2$ data show an increase.

## 5. Discussion

### 5.1. Model functioning

The one-dimensional model has proved to be very stable when run with varying source $Si(OH)_4$ concentrations. Modeled surface $Si(OH)_4$ and $NO_3$ concentrations agree well with field data and show the model to conform to a chemostat-like system with grazing setting most of the loss terms and the euphotic zone $Si(OH)_4$ responding with concentrations allowing growth rates of phytoplankton to equal loss rates. The occurrence of chronic low $Si(OH)_4$ concentrations relative to $NO_3$ in source waters (Ku et al., 1995) has been confirmed (Table 2). The one-dimensional model predicts correctly the result of this low source $Si(OH)_4$ condition; that surface $Si(OH)_4$ concentrations occupy a narrow range compared to a wider variation in surface $NO_3$, as in a chemostat with a limiting nutrient ($Si(OH)_4$) and varying feed-water concentrations of the non-limiting nutrient ($NO_3$).

### 5.2. Comparisons with field data

The one-dimensional model predicts distributions of $Si(OH)_4$ and $NO_3$ with depth varying with source $Si(OH)_4$ that match very well with JGOFS EqPac data and from areas to the west, analyzed by Dunne et al. (1999). These modeled profiles appear to be strongly correlated with the ratios of particulate Si:N measured in near-surface traps, and so confirm the Dunne et al. analysis and provide a prediction of changes in the quality of export flux with changes in source nutrients. Property–property plots, e.g. $Si(OH)_4$ vs. $NO_3$ and $TCO_2$ vs. $Si(OH)_4$ or $NO_3$ show breakpoints at the boundary between the source region (i.e. deep) and euphotic zone in both model output and JGOFS EqPac data. Similar breakpoints were observed in GEOSECS data by Broecker and Peng (1982). Although Broecker and Peng (1982)

interpreted these changes in slope of $TCO_2$ vs. $NO_3$ to be the result of $CO_2$ effusion to the atmosphere, the one-dimensional model shows a portion of the $TCO_2$ disappearance to be due to biological uptake and export. The modeled nitrogen uptake and $f$-ratio values correspond to JGOFS EqPac data most closely to the observations made in cruises in TT008 and TT012. Model over-estimates of $\rho NO_3$ compared to field data obtained during TT007 are likely the result of low upwelling activity in early 1992 (Kessler and McPhaden, 1995) and use of constant upwelling rates in the model runs. The one-dimensional model simulations agree closely with data obtained from the equatorial Pacific at 180°W (Leynaert et al., 2001), which include $Si(OH)_4$ uptake, $Si(OH)_4$ uptake kinetic experiments and biogenic silica values. The ambient surface $Si(OH)_4$ concentration measured by Leynaert et al. (2001) was close to the value of the half-saturation constant for $Si(OH)_4$ uptake, $K_{Si(OH)4}$. When $10\,mmol\,m^{-3}$ $Si(OH)_4$ was added to incubated samples, increased uptake occurred at all nine stations from 8°S to 7°N. These results provided direct evidence for $Si(OH)_4$ limitation of $Si(OH)_4$ uptake in equatorial Pacific waters.

### 5.3. Comparison with other models

Our one-dimensional model was developed specifically to understand the role of $Si(OH)_4$ in equatorial production and export of biogenic elements and is unique in that respect. Other existing equatorial models were developed from different viewpoints, e.g. the models of Loukos et al. (1997) and Leonard et al. (1999) do not include $Si(OH)_4$ as a variable and are oriented toward Fe as the limiting factor. The Loukos et al. (1997) model included only one phytoplankton and one zooplankton compartment and so had to be forced to low assimilation rates and high excretion rates to achieve the low $f$-ratio values known for the equator. Their model consequently gives new and regenerated production rates similar to the Dugdale and Wilkerson (1998) model and within the range of the present one-dimensional model (Table 6), and values for $CO_2$ export close to Dugdale and Wilkerson (1998) and slightly below the bottom of the range for the one-dimensional model (Table 6). Loukos et al. (1997) modified their N-limited condition to an Fe-limited condition with very little difference between the two outcomes except when Fe was made replete. The Leonard et al. (1999) model under-estimates by a large margin new and regenerated production and $f$-ratio, under simulated El Niño conditions compared to either field data or other models. The same model over-estimates greatly the same variables under non-El Niño conditions. Neither of these models provides information on $Si(OH)_4$ concentrations, Si production or export.

The only two equatorial models that can be directly compared are the present one-dimensional and the Dugdale and Wilkerson (1998) model, as both these separate out C, N, and Si processes. New and regenerated N production and $f$-ratio from Dugdale and Wilkerson (1998) fall within the ranges for the one-dimensional model (Table 6). Export of N, Si, and C from the Dugdale and Wilkerson (1998) model are close to or within the ranges given by the one-dimensional model.

### 5.4. Role of Fe

The present form of the one-dimensional model does not consider Fe as a variable, including it implicitly, however, by the initial slopes ($\alpha$) of the PI curves for the two phytoplankton groups set below optimum values (Chai et al., 2002). Agreement of model results with data reported here suggests that Fe is supplied by upwelling in adequate quantities to support the high phytoplankton growth rates measured in the equatorial Pacific (Chavez et al., 1991). Fe data for the upwelling zone are sparse, but when plotted against $NO_3$ show a positive slope with an $Fe = 0$ intercept at $NO_3 =$ about $10\,mmol\,m^{-3}$ (Takahashi, pers comm, Dunne et al., 1999; data from Johnson et al., 1997). Comparison of this intercept, $10\,mmol\,m^{-3}$, with the source $NO_3$ data in Table 2 indicates that Fe was supplied by upwelling during the JGOFS EqPac cruises with the possible exception of part of the TT008 cruise.

Table 6
Comparison of equatorial nutrient uptake rates and export rates resulting from the one-dimensional model and other equatorial models

| | $\rho NO_3$ (mmol $m^{-2} day^{-1}$) | $\rho NH_4$ (mmol $m^2 day^{-1}$) | $\rho N_{Total}$ (mmol $m^2 day^{-1}$) | $f$-ratio | PON export (mmol $m^{-2} day^{-1}$) | Si export (mmol $m^{-2} day^{-1}$) | POC export (mmol $m^{-2} day^{-1}$) |
|---|---|---|---|---|---|---|---|
| One-dimensional model | | | | | | | |
| Source $Si(OH)_4 = 3$ | 3.25 | 8.93 | 12.18 | 0.27 | 0.69 | 0.35 | 5.04 |
| Source $Si(OH)_4 = 7.5$ | 1.96 | 6.80 | 8.76 | 0.22 | 0.88 | 1.54 | 6.42 |
| Source $Si(OH)_4 = 15$ | 2.45 | 7.30 | 9.75 | 0.25 | 0.98 | 3.20 | 7.15 |
| Mean | | | | | 0.85 | 1.70 | 6.20 |
| Range | | | | | 0.69–0.98 | 0.35–3.20 | 5.04–7.15 |
| Dugdale and Wilkerson (1998) | | | | | | | |
| Source $Si(OH)_4 = 5.67$ | 2.36 | 9.2 | 11.56 | 0.2 | 0.76 | 2.36 | 5.01 |
| Leonard et al. (1999) | | | | | | | |
| El Niño | 0.15 | | 2.27 | 0.07 | | | |
| Non-El Niño | 8.48 | | 21.76 | 0.41 | | | |
| Loukos et al. (1997) | | | | | | | |
| NNPZD, annual mean | 2.42 | 10.91 | 13.3 | 0.18 | 1.36 | | 4.6 |
| Range | | | | | | | 4.0–4.9 |
| NNPZD-Fe, annual mean | 2.42 | 10.91 | 13.3 | 0.18 | 1.39 | | 4.8 |
| Range | | | | | | | 3.8–5.4 |

### 5.5. Significance

Since most models, including this one-dimensional model, of the equatorial ecosystem can be and have been tuned to approximate mean observed conditions, e.g. Chai et al. (1996), Loukos et al. (1997), the predictions over the full range of observed and likely conditions are more relevant than these "steady-state" or mean predictions. Perhaps the most interesting feature of the one-dimensional model is the stability brought about by the competitive interactions between the picoplankton, diatoms, micro- and meso-zooplankton. These interactions result in narrow ranges in many variables, e.g. total phytoplankton biomass, total N production (= primary production when multiplied by an appropriate C:N ratio), total new N production, value of $f$-ratio and surface silicate and nitrate concentrations, all of which are known to vary through narrow ranges in the equatorial Pacific upwelling system. The value of this one-dimensional, two phytoplankton, two zooplankton, $NO_3$, $NH_4$ and $Si(OH)_4$ (2PP, 2ZP, NNSi) model lies in its contribution to understanding the importance of the inner pathways of nutrient and energy, i.e. in the separation of picoplankton, diatoms, microzooplankton, mesozooplankton, and nutrient ($NO_3$, $NH_4$, and $Si(OH)_4$) processes, some of which have not been or little studied in the equatorial upwelling system, e.g. size fractionation of nitrogen uptake between picoplankton and diatoms, or $Si(OH)_4$ uptake and regeneration.

A model prediction of potential importance is the occurrence of a maximum surface $TCO_2$ when $Si(OH)_4$ concentration in the source water is 5 or 7.5 mmol $m^{-3}$, the latter value lying within the mean source concentrations observed in the JGOFS cruises, 6.57–9.96 mmol $m^{-3}$ (Table 2). In the one-dimensional model, this maximum in surface $TCO_2$ results from increasing diatom populations that support increased mesozooplankton populations and intensified grazing on picoplankton resulting in decreased $NO_3$ uptake by the picoplankton.

### 5.6. Role of diatoms

According to the results of the one-dimensional model, diatoms, although relegated to the minor phytoplankton biomass constituent, play a major role in the inner workings of the equatorial ecosystem, especially in maintaining the high level of stability characteristic of the system. Diatoms, depending on the supply of $Si(OH)_4$ from upwelling, may cause an increase in $CO_2$ flux to the atmosphere or a decrease, and may actually be the cause of the "normal" state of the equator as a net source to the atmosphere. Finally, diatoms appear in the equatorial system to be doing what they do best, in pumping $Si(OH)_4$ out of the euphotic zone leaving $NO_3$ behind in excess (Dugdale et al., 1995). The maximum ratio of Si:N export in the one-dimensional model is nearly 4:1, a ratio known for the drawdown of $Si(OH)_4$ and $NO_3$ in the Southern Ocean (Minas and Minas, 1992). A consequence of this effect is that sedimented biogenic silica is a sensitive indicator of changes in source concentration of $Si(OH)_4$ and the state of the ecosystem including $CO_2$ flux to the atmosphere. However, large changes in sedimented biogenic silica are correlated with smaller changes in new N and C production and N and C export production (Table 6). This means that sedimented biogenic silica under the equatorial upwelling area may be viewed as an amplifier of changes in surface properties.

These conclusions, of considerable interest to paleoceanographers and paleoclimatologists as well as biological oceanographers, rest to some extent on field data, but to a larger extent on our modeling results. When the one-dimensional model was first constructed there was no direct evidence for $Si(OH)_4$ limitation of diatom growth in the equatorial Pacific upwelling system. Recent direct measurements of $Si(OH)_4$ uptake kinetics in the Pacific equatorial upwelling system and a series of $Si(OH)_4$ enrichment experiments (Leynaert et al., 2001) have now confirmed the $Si(OH)_4$ limitation first proposed by Ku et al. (1995). The challenge now is to obtain measurements of key ecosystem parameters under a variety of source water concentrations and upwelling conditions. A question of first-order importance is whether the changes in surface $TCO_2$ at source concentrations simulated by the one-dimensional model occur in synchrony with changes in the diatom populations and whether these changes in turn occur in synchrony with changes in source $Si(OH)_4$ concentration.

## Acknowledgements

This research was supported by NSF Grant OCE-9802060 to R.C. Dugdale and F.P. Wilkerson. Two anonymous reviewers made comments that improved the final version of the manuscript. This publication is US JGOFS contribution number 696.

## References

Barber, R.T., Chavez, F.P., 1991. Regulation of primary productivity rate in the equatorial Pacific. Limnology and Oceanography 36 (8), 1803–1815.

Barber, R.T., Sanderson, M.P., Lindley, S.T., Chai, F., Newton, J., Trees, C.C., Foley, D.G., Chavez, F.P., 1996. Primary productivity and its regulation in the equatorial Pacific during and following the 1991–1992 El Niño. Deep-Sea Research II 43 (4–6), 933–969.

Bidigare, R.R., Ondrusek, M.E., 1996. Spatial and temporal variability of phytoplankton pigment distributions in the central equatorial Pacific Ocean. Deep-Sea Research II 43, 809–833.

Blain, S., Leynaent, A., Treguer, P., Chnetiennot-Dinet, M-J., Rodier, M., 1997. Biomass, growth rates and limitation of Equatorial Pacific diatoms. Deep-Sea Research 44, 1255–1275.

Broecker, W.S., Peng, T-H., 1982. Tracers in the Sea. Eldigio Press, New York.

Chai, F., Lindley, S.T., Barber, R.T., 1996. Origin and maintenance of a high $NO_3$ condition in the equatorial Pacific. Deep-Sea Research II 43, 1031–1064.

Chai, F., Dugdale, R.C., Peng, T.-H., Wilkerson, F.P., Barber, R.T., 2002. One-dimensional ecosystem model of the equatorial Pacific upwelling system. Part I: Model development and silicon and nitrogen cycle. Deep-Sea Research II 49, 2713–2743.

Chavez, F.P., Buck, K.R., Coale, K.H., Martin, J.H., DiTullio, G.R., Welshmeyer, N.A., Jacobson, A.C., Barber, R.T., 1991. Growth rates, grazing, sinking and iron limitation of equatorial Pacific phytoplankton. Limnology and Oceanography 36, 1816–1833.

Chavez, F.P., Buck, K.R., Service, S.K., Newton, J., Barber, R.T., 1996. Phytoplankton variability in the central and eastern tropical Pacific. Deep-Sea Research II 43, 835–870.

Coale, K.H., et al., 1996. A massive phytoplankton bloom induced by an ecosystem-scale iron fertilization experiment in the equatorial Pacific Ocean. Nature 838, 495–501.

Cullen, J.J., Lewis, M.R., Davis, C.O., Barber, R.T., 1992. Photosynthetic characteristics and estimated growth rates indicate grazing is the proximate control of primary production in the equatorial Pacific. Journal of Geophysical Research 97, 639–654.

Dugdale, R.C., Goering, J.J., 1970. Nutrient limitation and the path of nitrogen in Peru Current production. Anton Bruun Rep. #4 Texas A&M Press, pp. 5.3–5.8.

Dugdale, R.C., Wilkerson, F.P., 1998. Silicate regulation of new production in the equatorial Pacific upwelling. Nature 391, 270–273.

Dugdale, R.C., Wilkerson, F.P., Barber, R.T., Chavez, F.P., 1992. Estimating new production in the equatorial Pacific Ocean at 150°W. Journal of Geophysical Research 97, 681–686.

Dugdale, R.C., Wilkerson, F.P., Minas, H.J., 1995. The role of a silicate pump in driving new production. Deep-Sea Research 42, 697–719.

Dunne, J.P., Murray, J.W., Aufdenkampe, A.K., Blain, S., Rodier, M., 1999. Silicon–nitrogen coupling in the equatorial Pacific upwelling zone. Global Biogeochemical Cycles 13 (3), 715–726.

Feely, R.A., Wanninkhof, R., Goyet, C., Archer, D.E., Takahashi, T., 1997. Variability of $CO_2$ distributions and sea–air fluxes in the central and eastern equatorial Pacific during the 1991–1994 El Niño. Deep-Sea Research II 44 (9–10), 1851–1867.

Foley, D.G., Dickey, T.D., McPhaden, M.J., Bidigare, R.R., Lewis, M.R., Barber, R.T., Lindley, S.T., Garside, C., Manov, D.V., McNeil, J.D., 1997. Long waves and primary productivity variations in the equatorial Pacific at 0°, 140°W. Deep-Sea Research II 44, 1801–1826.

Frost, B.W., Franzen, N.C., 1992. Grazing and iron limitation in the phytoplankton stock and nutrient concentration: a chemostat analogue of the Pacific equatorial upwelling zone. Marine Ecology Progress Series 83, 291–303.

Iriarte, J.L., Fryxell, G.A., 1995. Micro-phytoplankton at the equatorial Pacific (140°W) during the JGOFS EqPac time series studies: March to April 1992. Deep-Sea Research II 42, 559–584.

Johnson, K.S., Gordon, R.M., Coale, K.H., 1997. What controls dissolved iron concentrations in the world ocean? Marine Chemistry 57, 137–161.

Kessler, W.S., McPhaden, M.J., 1995. The 1991–1993 El Niño in the central Pacific. Deep-Sea Research II 42, 295–333.

Ku, T.L., Luo, S., Kusakabe, M., Bishop, J.K.B., 1995. $^{228}$Ra-derived nutrient budgets in the upper equatorial Pacific and the role of "new" silicate in limiting productivity. Deep-Sea Research II 42, 479–497.

Landry, M.R., Barber, R.T., Bidigare, R.R., Chai, F., Coale, K.H., Dam, H.G., Lewis, M.R., Lindley, S.T., McCarthy, J.J., Roman, M.R., Stoecker, D.K., Verity, P.G., White, J.R., 1997. Iron and grazing constraints on primary production in the central equatorial Pacific: an EqPac synthesis. Limnology and Oceanography 42, 405–418.

Leonard, C.L., McClain, C.R., Murtugudde, R., Hofmann, E.E., Harding Jr., L.W., 1999. An iron-based ecosystem model of the central equatorial Pacific. Journal of Geophysical Research 104, 1325–1341.

Levitus, S., Conkright, M.E., Reid, J.L., Najjar, R.G., Mantyla, A., 1993. A distribution of nitrate, phosphate and silicate in the world oceans. Progress in Oceanography 31 (3), 245–273.

Leynaert, A., Treguer, P., Lancelot, C., Rodier, M., 2001. Silicon limitation of biogenic silica production in the equatorial Pacific. Deep-Sea Research I 48, 639–660.

Loukos, H., Frost, B., Harrison, D.E., Murray, J.W., 1997. An ecosystem model with iron limitation of primary production in the equatorial Pacific at 14°W. Deep-Sea Research II 44, 2221–2249.

McCarthy, J.J., Garside, C., Nevins, J.L., Barber, R.T., 1996. New production along 140°W in the equatorial Pacific during and following the 1992 El Nino event. Deep-Sea Research II 43, 1065–1093.

Minas, H.J., Minas, M., 1992. Net community production in "High Nutrient-Low Chlorophyll" waters of the tropical and Antarctic Oceans: grazing versus iron hypothesis. Oceanolgia Acta 15, 145–162.

Monod, J., 1950. La technique de la culture contnue: theorie at applications. Annales d'Institut Pasteur, Lille. 79, 390–410.

Murray, J.W., Johnson, E., Garside, C., 1995. A US JGOFS process study in the equatorial Pacific (EqPac): introduction. Deep-Sea Research II 42, 275–293.

Murray, J.W., Young, J., Newton, J., Dunne, J., Chapin, T., Paul, B., McCarthy, J.J., 1996. Export flux of particulate organic carbon from the central equatorial Pacific determined using a combined drifting trap—$^{234}$Th approach. Deep-Sea Research II 43, 1095–1133.

Peña, M.A., Lewis, M.R., Harrison, W.G., 1990. Primary productivity and size structure of phytoplankton biomass on a transect of the equator at 135°W in the Pacific Ocean. Deep-Sea Research 37, 295–315.

Philander, S.G., 1990. El Niño, La Niña and the Southern Oscillation.Academic Press, Inc., New York, pp. 293.

Price, N.M., Ahner, B.A., Morel, F.M.M., 1994. The equatorial Pacific Ocean: grazer controlled phytoplankton populations in an iron-limited ecosystem. Limnology and Oceanography 39, 520–534.

Raimbault, P., Slawyk, G., Boudjellal, B., Coatanoan, C., Conan, P., Coste, B., Garcia, N., Moutin, T., Pujo-Pay, M., 1999. Carbon and nitrogen uptake and export in the equatorial Pacific at 150°W: evidence of an efficient regenerated production cycle. Journal of Geophysical Research 104, 3341–3356.

Rodier, M., Le Borgne, R., 1997. Export flux of particles at the equator in the western and central Pacific Ocean. Deep-Sea Research II 44, 2085–2113.

Sanderson, M.P., Hunter, C.N., Fitzwater, S.E., Gordon, R.M., Barber, R.T., 1995. Primary productivity and trace metal contamination measurements from a clean rosette system versus ultra-clean Go-Flo bottles. Deep-Sea Research II 42, 431–441.

Walsh, J.J., 1976. Herbivory as a factor in patterns of nutrient utilization in the sea. Limnology and Oceanography 21, 1–13.

Wyrtki, K., 1981. An estimate of equatorial upwelling in the Pacific. Journal of Physical Oceanography 11, 1205–1214.